Computers and Concrete, Vol. 1, No. 4 (2004) 433-455
DOI: http://dx.doi.org/10.12989/cac.2004.1.4.433

Numerical simulations of localization of deformation in quasi-brittle materials within non-local softening plasticity

J. Bobinski† and J. Tejchman‡

Civil Engineering Department, Gdansk University of Technology, 80-952 Gdansk, Narutowicza 11/12, Poland
(Received January 5, 2004, Accepted November 10, 2004)

Abstract. The paper presents results of FE-calculations on shear localization in quasi-brittle materials during both an uniaxial plane strain compression and uniaxial plane strain extension. An elasto-plastic model with a linear Drucker-Prager type criterion using isotropic hardening and softening and non-associated flow rule was used. A non-local extension was applied in a softening regime to capture realistically shear localization and to obtain a well-posed boundary value problem. A characteristic length was incorporated via a weighting function. Attention was focused on the effect of mesh size, mesh alignment, non-local parameter and imperfections on the thickness and inclination of shear localization. Different methods to calculate plastic strain rates were carefully discussed.

Keywords: brittle material; compression; extension; material softening; non-locality; plasticity; shear localization.

1. Introduction

Failure in most engineering materials like metals, soils, rocks, polymers and concrete is proceeded by the occurrence of narrow zones of intense deformation. Due to these zones, a degradation of the material strength develops. The localization of deformation can occur as cracks (mode I) or shear zones (mode II). An understanding of the mechanism of the formation of localization is of a crucial importance since they act as a precursor to ultimate fracture and failure. In order to properly analyze the failure behavior of materials, the phase of the localization of deformation has to be modeled in a physically consistent and mathematically correct manner. Classical FE-analyses within a continuum mechanics are not able to describe properly both the thickness of localized zones and distance between them since they do not include a characteristic length of microstructure. Thus, they suffer from a pathological dependence on the fineness of the spatial discretisation (its size and orientation) because differential equations of motion change their type (from elliptic to hyperbolic during quasi-static calculations) and the rate boundary value problem becomes mathematically ill-posed (Mühlhaus 1986, de Borst, *et al*. 1992). The deformations tend to localize in a zero thickness zone in an analytical analysis and in one element wide region in FE-calculations (the strain-softening domain is limited to a point and no energy dissipation takes place). As a result, the computed load-

† Research Fellow
‡ Professor

displacement curves are severely mesh dependent (in particular, in a post-peak regime). Thus, classical constitutive laws require an extension by a characteristic length to accurately capture the formation of localization of deformation, to obtain an objective solution upon mesh refinement and to take into account microscopic inhomogeneities triggering shear localization (e.g., aggregate size).

The intention of the paper was to analyze localization of deformations in quasi-brittle materials (e.g., concrete-like materials) in the form of spontaneous shear localization. The analyses were performed using a finite element method and an elasto-plastic law with isotropic hardening and non-local softening. Due to the presence of a characteristic length, the law can describe the formation of localization of deformations with a certain thickness and spacing. The FE-results converge to a finite size of a shear zone via mesh refinement, and initial and boundary value problems become mathematically well-posed at the onset of localization.

The FE-calculations were carried out with brittle specimens subjected to both uniaxial plane strain compression and extension. Special attention was laid on the influence of the orientation of the mesh on the inclination of a spontaneous shear zone in the specimen. In addition, the effect of the imperfection, characteristic length, non-local parameter and geometric non-linearity was analyzed. Different methods to calculate non-local strain rates were discussed. The way of the implementation of a non-local model in a commercial finite element code was described. An unique relationship between the width of the shear zone and the characteristic length was proposed. Advantages and disadvantages of the non-local model were outlined.

2. Material behaviour

The behaviour of quasi-brittle materials is very complex due to their heterogeneous structure, strong anisotropy, non-linearity and interaction between friction and cracking. Usual quasi-brittle materials are characterised by the following properties:

- the compressive strength is several times higher than the tensile one,
- the strength increases with increasing confining pressure and loading velocity,
- the shape of the failure surface in a principle stress space is close to paraboloidal,
- the shape of the failure surface in deviatoric planes changes from a curvilinear triangle with smoothly rounded corners to nearly circular with increasing pressure,
- the initial volume change in the form of compaction is almost linear up to the critical stress, later volumetric expansion (dilatancy) occurs,
- the curvature of the failure surface is produced by interaction between dilatancy and crushing,
- the curved meridians in planes containing the hydrostatic axis are different for compression and extension,
- the non-associated flow rule prevails,
- the ductile damage occurs at high pressures and brittle (unstable) one at low pressures,
- localization of deformation can occur in the form of shear zones (if friction dominates) and cracks (if cohesion is dominant),
- the stiffness degradation due to localization of deformation occurs,
- scale effects expressed by increasing strength with increasing aggregate size and decreasing structure size exist.

To describe the behaviour of quasi-brittle materials, different models have been developed: continuum ones within fracture mechanics (Bazant and Cedolin 1979, Hillerborg 1986), damage mechanics (Dragon and Mróz 1979, di Prisco and Mazars 1996, Chen 1999, Ragueneau, *et al.* 2000), plasticity (Willam and Warnke 1975, de Borst 1986, Pietruszczak, *et al.* 1988, Menetrey and Willam 1995, Lade and Jakobsen 2002), coupled damage and plasticity (Lemaitre 1985, Ibrahimbegovic, *et al.* 2003) and discrete ones using a lattice approach (Herrmann, *et al.* 1989, Vervuurt, *et al.* 1994) and DEM (Sakaguchi and Mühlhaus 1997, Donze, *et al.* 1999, Place and Mora 2001).

To take into account localization of deformation with a certain thickness and spacing, a characteristic length (depending on the size of material heterogeneities) has to be included. It can be introduced with micro-polar (Mühlhaus 1986, Sluys 1992, Tejchman and Wu 1993, Tejchman, *et al.* 1999), strain gradient (Zbib and Aifantis 1989, Sluys 1989, Mühlhaus and Aifantis 1991, Pamin 1994, Sluys and de Borst 1994, Peerlings, *et al.* 1998, Meftah and Reynouard 1998, Pamin and de Borst 1998, Chen, *et al.* 2001, Zhou, *et al.* 2002, Askes and Sluys 2003), viscous (Sluys 1992, Loret and Prevost 1990) and non-local (Bazant 1986, Bazant and Lin 1988, Brinkgreve 1994, Strömberg and Ristinmaa 1996, Chen 1999, Marcher and Vermeer 2001, Maier 2002, di Prisco, *et al.* 2002, Jirasek and Rolshoven 2003) theories.

In a non-local theory, a variable which controls material softening is defined as an average quantity over a domain whose size is related to a material heterogeneity (i.e., it depends also upon variables in the next neighborhood). First non-local formulations were given by Eringen for elasticity (Eringen 1972) and plasticity (Eringen 1981). Next, Bazant (1986) formulated a fully non-local elasto-plastic model to describe the behaviour of concrete. Later, Bazant, *et al.* (1987), and Bazant and Lin (1988) used a partially non-local model within elasto-plasticity and damage mechanics (only some material variables were assumed to be non-local). The characteristic length was taken as $3 \times d_a$ (d_a – maximum size of the aggregate in concrete). Brinkgreve (1994), Schanz (1998) and Marcher and Vermeer (2001) analysed the behaviour of soils with an elasto-plastic model with non-local softening where only an effective strain measure was non-local. The characteristic length was related to a mean grain diameter d_{50} and was found to be $5 \times d_{50}$ (Marcher and Vermeer 2001). To obtain an uniform distribution of non-local plastic strains in a localized zone, Brinkgreve (1994) proposed a modification of a non-local model (the non-local strain measure included a local and non-local part). Maier (2002, 2003) and Tejchman (2003, 2004) applied a non-local hypoplastic law for granulates wherein only the modulus of deformations was treated non-locally. The characteristic length was related to a mean grain diameter of granulates d_{50} and was found to be approximately $2 \times d_{50}$. Strömberg and Ristinmaa (1996) developed an algorithm for an exact determination of non-local plastic strains in a von Mises material. In particular, non-local models were often used in damage mechanics (Pijaudier-Cabot and Bazant 1987, Pijaudier-Cabot 1995, di Prisco and Mazars 1996, Chen 1999, Ganghoffer and de Borst 2000).

3. Constitutive law

To check the capability of a non-local model to capture localization of deformation in quasi-brittle materials in the form of shear zones (mode II), in the first step, an elasto-plastic material model with a linear Drucker-Prager type criterion using isotropic hardening, isotropic non-local softening and non-associated flow rule was used. The yield function f assumed was similar to a compression

yield surface given in Abaqus (2001).

$$f = q + \mu \bullet p - \sigma_y(\kappa) \tag{1}$$

where q – von Mises equivalent stress, p – mean stress, $\mu = \tan\varphi$ - mobilised friction factor, φ – angle of internal friction, σ_y – cohesion yield stress and κ – hardening (softening) parameter. The yield condition $f = 0$ describes a cone in the principle stress space (the coefficient μ indicates the steepness of the cone). The equivalent stress q was defined as:

$$q = \sqrt{\frac{3}{2} s_{ij} s_{ij}} \tag{2}$$

where s_{ij} are deviatoric stresses. The mean stress p was:

$$p = \frac{\sigma_{ii}}{3} \tag{3}$$

The parameter κ, equal to the equivalent plastic strain ε_p was:

$$\varepsilon_p = \sqrt{\frac{2}{3} e_{ij}^p e_{ij}^p} \tag{4}$$

wherein e_{ij}^p – deviatoric plastic strains. The model uses a non-associated flow rule. The potential function g was chosen as:

$$g = q + \beta \bullet p \tag{5}$$

where $\beta = \tan\psi$ is the mobilised dilatancy (contractancy) factor and ψ is the dilatancy (contractancy) angle (sign "+" denotes dilatancy). For the parameters $\varphi = 0$ and $\psi = 0$, a von Mises yield criterion is obtained. In FE-analyses, the elastic modulus was taken as $E = 29$ GPa and Poisson's ratio as $v = 0.18$ (softening modulus $H = 0.8$ GPa), Fig. 1. The maximum cohesion yield stress was assumed to be $\sigma_y^{\max} = 32$ MPa at $\varepsilon_p = 0.11\%$. To simplify the FE-calculations, the mobilised internal friction angle φ was equal to 25° and the dilatancy angle ψ was taken as 10°.

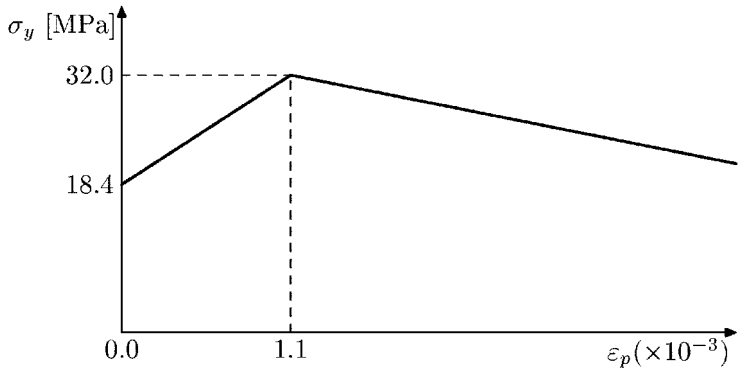

Fig. 1 Relationship between cohesion yield stress σ_y and equivalent plastic strain ε_p in a compressive regime

4. Non-local model

A non-local approach takes into account the fact that the evolution of the micro-structure at one point naturally influences the surrounding points during formation of localization. It was also proposed to obtain a well-posed boundary value problem, to ensure a mesh-independent solution and to promote convergence of a numerical calculation in a softening regime. It is based on a spatial averaging of tensor or scalar state variables in a certain neighbourhood of a given point (i.e., material response at a point depends both on the state of its neighbourhood and the state of the point itself). Thus, a characteristic length can be incorporated and softening can spread over material points. It is in contrast to a classical continuum mechanics, wherein the principle of local action holds (i.e., the dependent variables in each material point depend only upon the values of the independent variables at the same point), and softening at one material point does not affect directly the yield surfaces of other points.

A full non-local model involves a relationship between average stresses and average strains:

$$\sigma_{ij}^{*} = \frac{1}{A}\iiint w(x_n')\,\sigma_{ij}(x_n + x_n')\,dx_1'dx_2'dx_3' \tag{6}$$

$$\varepsilon_{ij}^{*} = \frac{1}{A}\iiint w(x_n')\,\varepsilon_{ij}(x_n + x_n')\,dx_1'dx_2'dx_3' \tag{7}$$

wherein a superimposed star denotes a non-local quantity, x_n is a global coordinate, x_n' is a local coordinate with $n = 1,2,3$, $w(x_n')$ denotes a weighting function and A stands for a weighted volume of the body:

$$A = \iiint w(x_n')\,dx_1'dx_2'dx_3' \tag{8}$$

In homogeneous materials, Eqs. (6) and (7) can be simplified to:

$$\sigma_{ij}^{*} = \frac{1}{A}\int w(r)\,\sigma\,dV \tag{9}$$

and

$$\varepsilon_{ij}^{*} = \frac{1}{A}\int w(r)\,\varepsilon\,dV \tag{10}$$

wherein r is the distance from the material point considered to other integration points of the entire material body. Usually, the error density function (normal Gaussian distribution function) is used as a weighting function w (which defines the averaging type):

$$w(r) = \frac{1}{l\sqrt{\pi}}\,e^{-\left(\frac{r}{l}\right)^2} \tag{11}$$

and

$$\int_{-\infty}^{\infty} w(r)\,dr = 1 \tag{12}$$

The parameter l denotes a characteristic length related to the micro-structure of the material (e.g.,

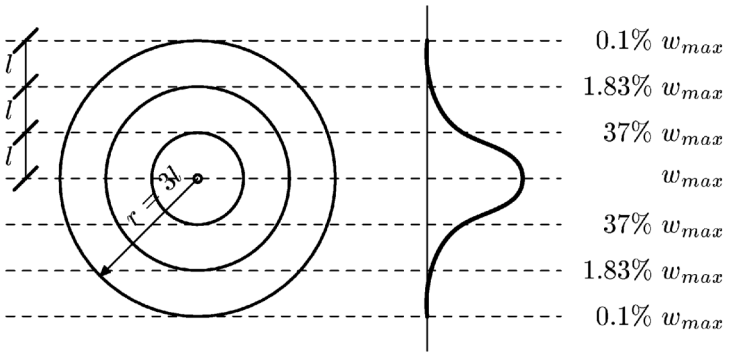

Fig. 2 Region of the influence of a characteristic length l and weighting function w

maximum aggregate size). At the distance of a few times the length l, the function w is equal to zero (Fig. 2). Other functions can be also chosen (Akkermann 2000, di Prisco, *et al.* 2002).

Usually, it is sufficient when the non-locality is related only to one state variable influencing the behaviour of the material in a softening regime (e.g., equivalent plastic strain measure or yield function). In our model, the non-locality was related to an equivalent plastic strain measure ε_p in the softening regime according to the Brinkgreve's proposal (1994) (i.e., stresses, strains and other variables remained local):

$$\varepsilon_p^*(x) = (1-\alpha)\varepsilon_p(x) + \frac{\alpha}{A}\int_{-\infty}^{\infty} w(r)\varepsilon_p(x+r)dV \tag{13}$$

where α denotes a non-local parameter controlling the size of the localized plastic zone and the distribution of plastic strain. For the parameter $\alpha = 0$, a local model is obtained, and for $\alpha = 1$, a classical non-local model (Bazant and Lin 1988) is recovered. When the non-local parameter $\alpha > 1$, the influence of non-locality increases and the localized plastic region reaches a finite mesh-independent size (Section 6). Brinkgreve (1994) derived an analytical formula for the thickness of a localized zone in an one-dimensional bar during tension with necking using a modified non-local approach by Eq. (13). According to this formula, if the non-local parameter was $\alpha = 1$, the thickness of the localized zone was equal to zero (similarly as in a local approach). During a FE-analysis, the integral in Eq. (13) was replaced by a summation operator. Thus, Eq. (13) became:

$$\varepsilon_p^*(x_i) = (1-\alpha)\varepsilon_p(x_i) + \alpha\frac{\sum_{j=1}^{np} w(|x_i - x_j|)\varepsilon_p(x_j)A_j}{\sum_{j=1}^{np} w(|x_i - x_j|)A_j} \tag{14}$$

where np is the number of all integration points in the whole body, x_j stand for co-ordinates of the integration point in each element and A_j is the actual element area.

A numerical problem in non-local models is the way how to calculate non-local terms since the plastic rates (unknown in advance) occur on both sides of Eq. (13). The plastic strain rates can be approximated by the total strain rates $d\varepsilon$ (Brinkgreve 1994):

$$d\varepsilon_p^*(x) \approx d\varepsilon_p(x) + \alpha\left(\frac{1}{A}\int_V w(r)d\varepsilon(x+r)dV - d\varepsilon(x) \right) \tag{15}$$

or calculated iteratively in an exact way according to the algorithm given by Strömberg and Ristinmaa (1996). The strain rates can be calculated in all integration points of the specimen, in the integration points where only plastic strains occur or only in the integration points where both plastic strains and softening simultaneously occur.

5. FE-implementation

Plane strain FE-calculations were performed with a specimen $b = 4$ cm wide and $h = 14$ cm high subject to uniaxial compression or uniaxial extension (Fig. 3). All nodes at the lower edge were fixed in a vertical direction. To preserve the stability of the specimen, the node in the middle of the lower edge was kept fixed. The deformations were initiated through constant vertical displacement increments prescribed to nodes along the upper edge of the specimen. The lower and upper edge were smooth. The standard boundary conditions of the classical continuum theory were used along the specimen's edges.

In the simulations, the localization was induced by one small material imperfection in the form of a weak element at mid-height of the specimen side (where the cohesion yield stress at peak $\sigma_y^{\max}$ of Fig. 1 was diminished by 2%). In addition, the calculations were carried out with three initial weak elements of a different size and spacing and with one initial strong element (where the cohesion yield stress at peak $\sigma_y^{\max}$ was increased by 2%).

To investigate the effect of the mesh size on the results, various discretisations were used: coarse (8×28), medium (16×56) and fine (24×84) where each quadrilateral was composed of four diagonally crossed triangular elements with linear shape functions (mesh inclination against the bottom was ($\theta = 45^o$). To examine the influence of the mesh alignment on the results, two other types of meshes were used: with a mesh inclination θ smaller than 45°: $\theta = 26.6^o$ (8×56), $\theta = 36.9^o$ (12×56), $\theta = 33.7^o$ (16×84) and $\theta = 39.8^o$ (20×84), and with a mesh inclination θ greater than 45°: $\theta = 56.3^o$ (12×28), $\theta = 63.5^o$ (16×28), $\theta = 51.3^o$ (20×56) and $\theta = 56.3^o$ (24×56).

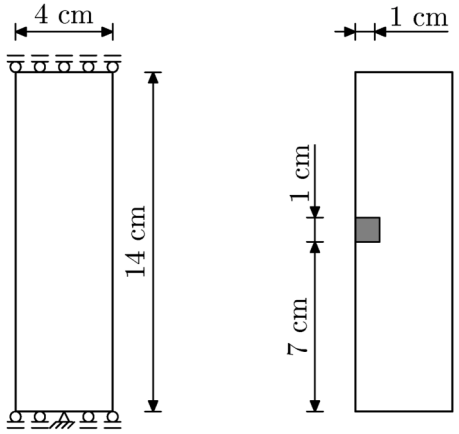

Fig. 3 Geometry of the specimen, boundary conditions and location of the imperfection

The non-local model was implemented in the commercial finite element code Abaqus (2001) for efficient computations. Such implementation can be performed with two methods. In the first method, two identical overlapping meshes are used. The first mesh allows to gather the information about coordinates of integration points in the entire specimen, area of all finite elements and total strain rates in each element. The elements in this mesh are defined by the user in the UEL procedure. They do not influence the results of stresses in the specimen body since they have no stiffness. The information stored is needed to calculate non-local variables with the aid of the second mesh which includes standard elements from the Abaqus library. The constitutive law is defined by the UMAT procedure. During odd iterations, the information is gathered in the elements of the first mesh. During even iterations, the stresses in the elements of the second mesh (including standard elements) are determined with taking into account non-local variables and a non-linear finite element equation is solved. Between odd and even iterations, the same element configuration is imposed. In the second method, only one mesh is used which contains user's elements (defined by the UEL procedure). During odd iterations, the information about the elements is stored, and during even iterations, the stresses within a non-local theory are determined. As compared to the first method, the second one consumes less time. However, it is less comfortable for the user due to the need of the definition of the stiffness matrix and out-of-balance load vector in finite elements.

For the solution of the non-linear equation of motion governing the response of a system of finite elements, a modified Newton-Raphson scheme with was used. The calculations were performed with a symmetric elastic global stiffness matrix. The calculations with a full Newton-Raphson method resulted in a poor convergency in the softening regime due to the fact that the determination of a tangent stiffness matrix within a non-local theory is virtually impossible. The following convergence criteria were assumed (Abaqus 2001):

$$r_{\max} \leq 0.01\,\tilde{q} \quad \text{and} \quad c_{\max} \leq 0.01\,\Delta u_{\max} \tag{16}$$

where $r_{\max}$ – the largest residual out-of-balance force, $\tilde{q}$ – spatial averaged force over the entire body, $c_{\max}$ – the largest correction of the displacement and $\Delta u_{\max}$ – the largest change of the displacement in the increment. The procedure yielded a sufficiently accurate and fast convergence. The magnitude of the maximum out-of-balance force at the end of each calculation step was smaller than 1% of the calculated total vertical force on the top of the specimen. The calculations with smaller tolerances (Eq. 16) did not influence the FE-results. The integration was performed in one sample point of each element (centroid).

To satisfy the consistency condition $f = 0$, the trial stress method (linearised expansion of the yield condition about the trial stress point) using an elastic predictor and a plastic corrector with return mapping algorithm (Ortiz and Simo 1986) was applied with the following criterion:

$$r_\lambda / \sigma_y^{\max} \leq 10^{-6} \tag{17}$$

where r_λ is the residual plastic multiplier and $\sigma_y^{\max}$ denotes the maximum cohesion yield stress in each increment.

The calculations were carried out using a large-displacement analysis available in the Abaqus finite element code (2001). In this method, the actual configuration of the body was taken into account. The Cauchy stress was taken as the stress measure. The conjugate strain rate was the rate of deformation. The rotation of the stress and strain tensor was calculated with the Hughes-Winget (1980) method.

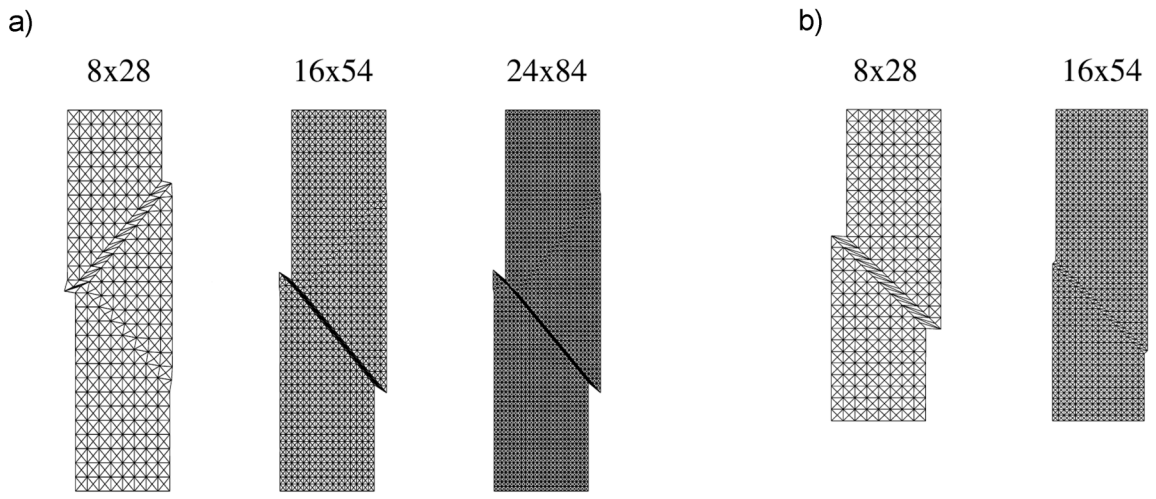

Fig. 4 Deformed meshes (local model $\alpha = 0$): a) $\varphi = 0^o$ and $\psi = 0^o$, b) $\varphi = 25^o$ and $\psi = 10^o$

6. FE-results

6.1. Effect of mesh size and mesh alignment

First, a local conventional elasto-plastic analysis was carried out during uniaxial compression. Fig. 4 shows deformed meshes for various discretisations ($\theta = 45^o$) with $\varphi = 0^o$ and $\psi = 0^o$ (Fig. 4a) and $\varphi = 25^o$ and $\psi = 10^o$ (Fig. 4b).

The deformations localize always in one element wide shear zone with an inclination of 45^o. The load-displacement curves are strongly dependent upon the discretisation size in the softening regime.

Figs. 5-8 depict the FE-results with an elasto-plastic model with non-local softening during uniaxial compression (with mesh alignment $\theta = 45^o$). As compared to the conventional elasto-plastic analysis, two additional constants were taken into account: the non-local parameter $\alpha = 2$ and characteristic length $l = 7.5$ mm. The calculated deformed meshes and non-local equivalent plastic strains are shown in Fig. 5. The load – displacement diagrams are presented in Fig. 6. In turn, Fig. 7 demonstrates the distribution of the equivalent plastic strains across the shear zone. The evolution of the equivalent non-local plastic strain is shown in Fig. 8.

During compression, two shear zones are simultaneously created expanding outward from the weak element on the left side (Fig. 8). They occur directly before the peak of the resultant vertical force on the top. After the peak, and up to the end, only one shear zone dominates. The complete shear zone is noticeable shortly after the peak. The shear zone is wider than one finite element (Fig. 5). The thickness of a shear zone is approximately $L = 2.4$ cm $(3.2 \times l)$ and does not depend upon the mesh size. The inclination of the shear zone against the bottom is equal to $\Theta = 44.8^o$, 44.8^o and 46.8^o with a coarse, medium and fine mesh, respectively. These values are in a good agreement with an inclination of a shear zone ($\Theta = 46^o$) obtained from an analytical formula based on a bifurcation theory (Sluys 1992):

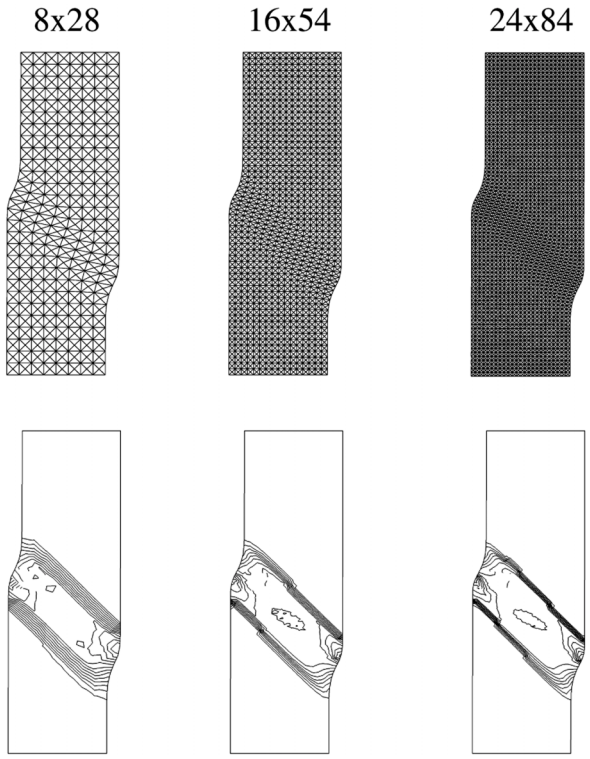

Fig. 5 Deformed meshes and contours of non-local equivalent plastic strains (non-local model, $\alpha = 2$, $l = 7.5$ mm, $\varphi = 25^{o}$ and $\psi = 10^{o}$)

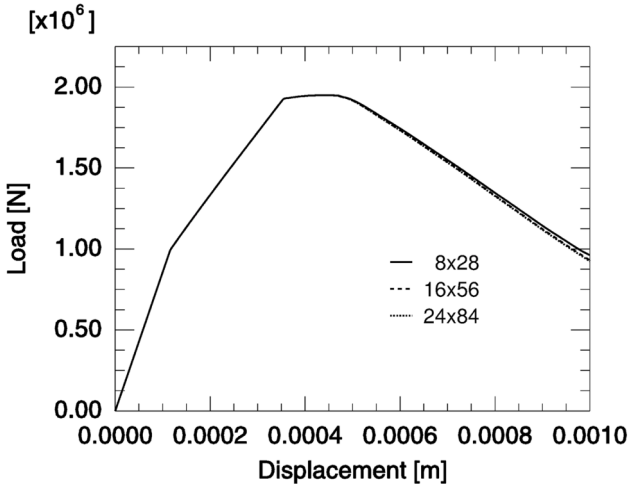

Fig. 6 Load-displacement curves (non-local model, $\alpha = 2$, $l = 7.5$ mm, $\varphi = 25^{o}$ and $\psi = 10^{o}$)

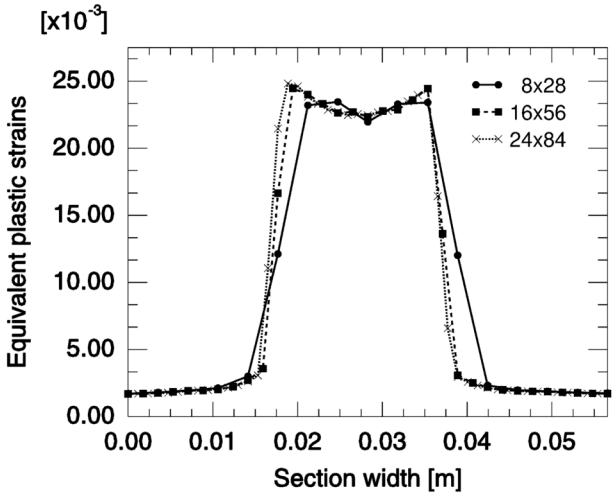

Fig. 7 Non-local equivalent plastic strains in a shear zone (non-local model, $\alpha = 2$, $l = 7.5$ mm, $\varphi = 25^{\circ}$ and $\psi = 10^{\circ}$)

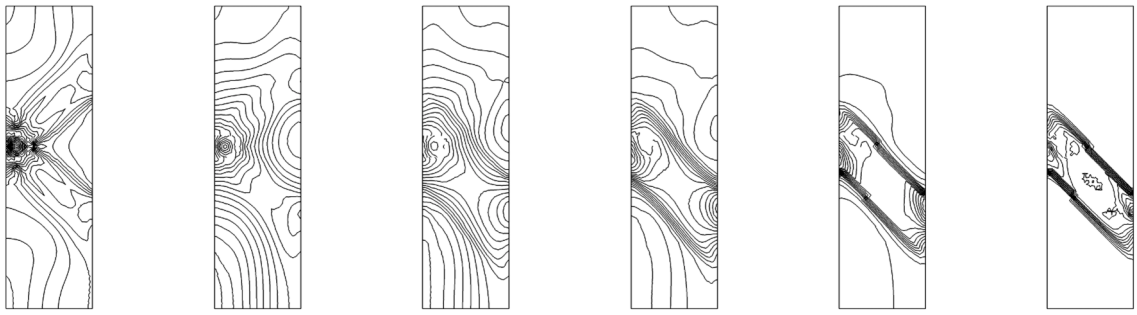

Fig. 8 Evolution of non-local equivalent plastic strains in the specimen during uniaxial compression (non-local model, $\alpha = 2$, $l = 7.5$ mm, $\varphi = 25^{\circ}$ and $\psi = 10^{\circ}$)

$$\tan^2\Theta = -\frac{9(s_1 + \nu s_3) + (1+\nu)\sqrt{3J_2}(\mu + \beta)}{9(s_2 + \nu s_3) + (1+\nu)\sqrt{3J_2}(\mu + \beta)} \tag{18}$$

where s_1, s_2 and s_3 are components of the deviatoric principle stress tensor, J_2 denotes the second invariant of the deviatoric stress tensor and ν is the Poisson's ratio. The calculated inclinations of the shear zone against the bottom (using medium mesh) with other values of φ and ψ: $\varphi = 40^{\circ}$ and $\varphi = 10^{\circ}$, and $\varphi = 40^{\circ}$ and $\psi = 25^{\circ}$ were equal to 48.6° and 52.0°, respectively. These values again agree well with Eq. (18) (48.1° and 50.2°, respectively). The growth of the internal friction angle and dilatancy angle obviously increases the inclination of the shear zone.

The evolution of the vertical force along the top before and after the peak is the same for various discretisations (Fig. 6). The maximum vertical force, 1.95 MN (corresponding to the compressive strength 49 MPa), occurs at the vertical displacement of 0.4 mm. The distribution of non-local

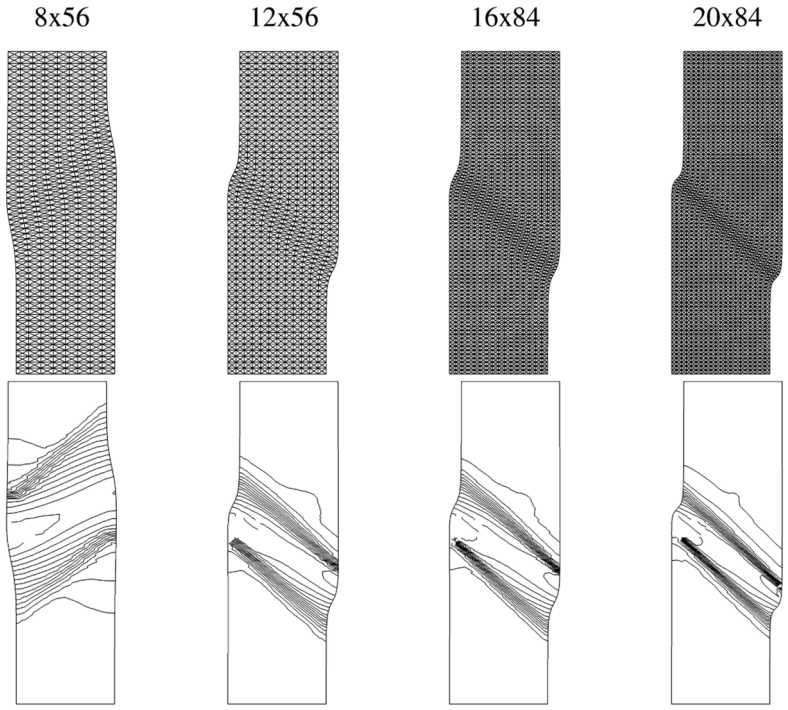

Fig. 9 Deformed meshes and contours of non-local equivalent plastic strains (non-local model, $\theta < 45^o$, $\alpha = 1$, $l = 20$ mm, $\varphi = 25^o$ and $\psi = 10^o$)

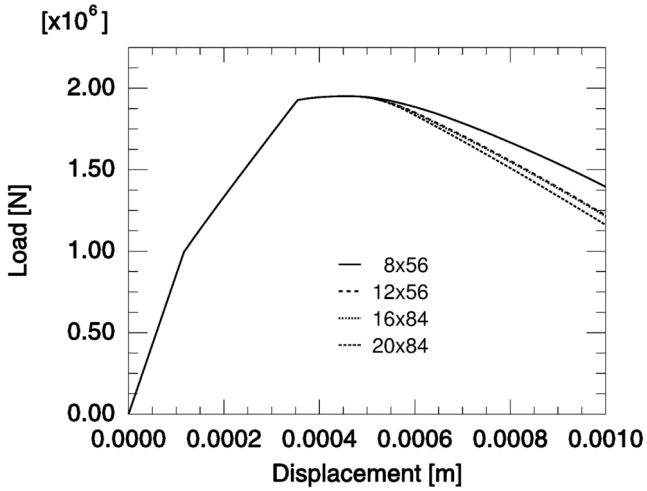

Fig. 10 Load-displacement curves (non-local model, $\theta < 45^o$, $\alpha = 1$, $l = 20$ mm, $\varphi = 25^o$ and $\psi = 10^o$)

equivalent plastic strains in a section perpendicular to the shear zone is fully uniform (Fig. 7). Due to that the non-local parameter is larger than 1, the difference between the non-local and local plastic strains (Eq. 13) results in a constant value of the plastic strains (Jirasek and Rolshoven

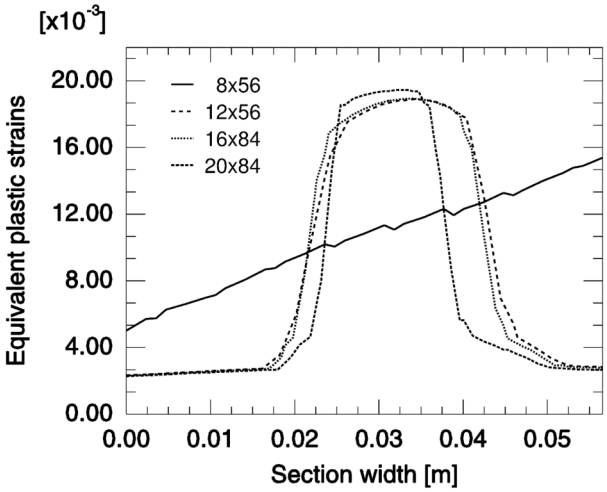

Fig. 11 Distribution of non-local equivalent plastic strains in a shear zone (non-local model, $\theta < 45^{\circ}$, $\alpha = 1$, $l = 20$ mm, $\varphi = 25^{\circ}$ and $\psi = 10^{\circ}$)

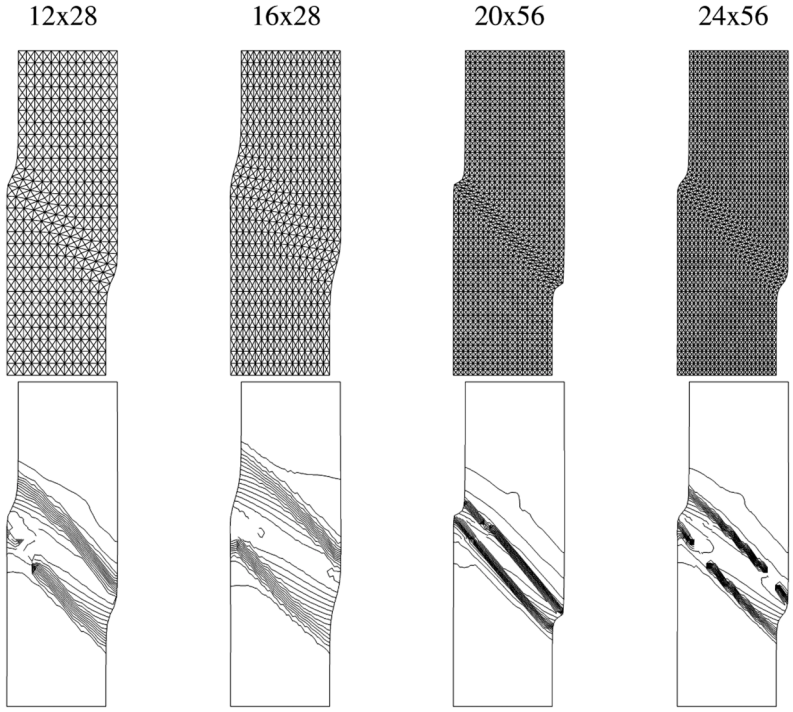

Fig. 12 Deformed meshes and contours of non-local equivalent plastic strains with various meshes (non-local model, $\theta > 45^{\circ}$, $\alpha = 1$, $l = 20$ mm, $\varphi = 25^{\circ}$ and $\psi = 10^{\circ}$)

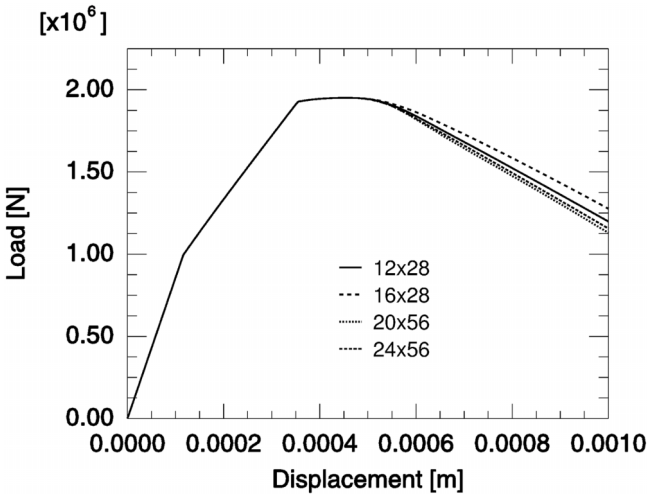

Fig. 13 Load-displacement curves (non-local model, $\theta > 45^o$, $\alpha = 1$, $l = 20$ mm, $\varphi = 25^o$ and $\psi = 10^o$)

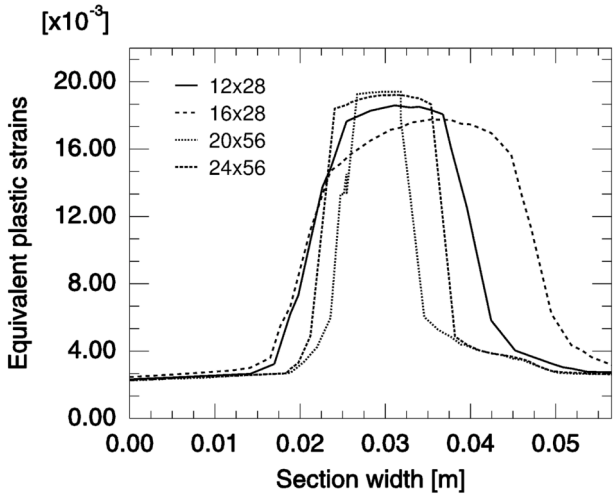

Fig. 14 Distribution of non-local equivalent plastic strains in a shear zone (non-local model, $\theta > 45^o$, $\alpha = 1$, $l = 20$ mm, $\varphi = 25^o$ and $\psi = 10^o$)

2003). Separately, the non-local and local plastic strains have an exponential shape.

The FE-calculations were also performed with a mesh alignment lower than 45°. The width of the shear zone was equal to $L = 2.4$ cm for all meshes except for the coarsest one (8×56) where the localization zone was equal to $L = 3.6$ cm. The inclination of the shear zone was: $\Theta = 44.0^o$ (8×56, $\theta = 26.6^o$), $\Theta = 43.9^o$ (12×56, $\theta = 36.9^o$), $\Theta = 47.6^o$ (16×84, $\theta = 33.7^o$) and $\Theta = 45.2^o$ (20×84, $\theta = 39.8^o$). The load–displacement diagrams were similar using all mesh discretisations. In the FE-studies assuming a mesh inclination greater than 45°, the width of the shear zone was again 2.4 cm with the meshes 20×56 and 24×56, and 2.9 cm with the meshes 12×28 and 16×28. The

inclination of the shear zone was 50.3° (12×28, $\theta = 56.3°$), 47.2° (16×28, $\theta = 47.2°$), 50.1° (20×56, $\theta = 50.1°$) and 49.1° (24×56, $\theta = 56.3°$).

The FE-results showed that the evolution of the vertical force along the top and thickness of the spontaneous shear zone did not depend upon mesh refinement within a modified non-local continuum. The effect of the mesh alignment on the inclination of the shear zone was negligible.

The FE-results with a classical non-local model, $\alpha = 1$, (Bazant and Lin 1988) are demonstrated in Figs. 9-11 (using meshes with an inclination lower θ than 45°), and in Figs. 12-14 (using meshes with an inclination θ greater than 45°). The calculations show that the results are only partly mesh-independent. The evolution of the vertical force on the top edge was only slightly different in a softening regime (Figs. 10 and 13). However, the width of the localized zone was different: $L = 2.7$ cm (12×56 and 16×84) and $L = 1.9$ cm (20×84) at $\theta < 45°$ (Fig. 11). The shear zone using a mesh 8×56 was very wide and had an opposite direction. The inclination of the shear zone was similar: $\Theta = 43.6°$ (12×56, $\theta = 36.9°$), $\Theta = 43.8°$ (16×84, $\theta = 33.7°$) and $\Theta = 45.5°$ (20×84, $\theta = 39.8°$). When the mesh alignment was larger than 45°, the width of the shear zone was again different: $L = 2.7$ cm, 3.3 cm, 1.2 cm and 1.7 cm for meshes 12×28, 16×28, 20×56 and 24×56 mesh, respectively (Fig. 12). Its inclination was varied: $\Theta = 55.2°$ (12×28, $\theta = 56.3°$), $\Theta = 47.5°$ (16×28, $\theta = 47.2°$), $\Theta = 51.3°$ (20×56, $\theta = 50.1°$) and $\Theta = 50.6°$ (24×56, $\theta = 56.3°$).

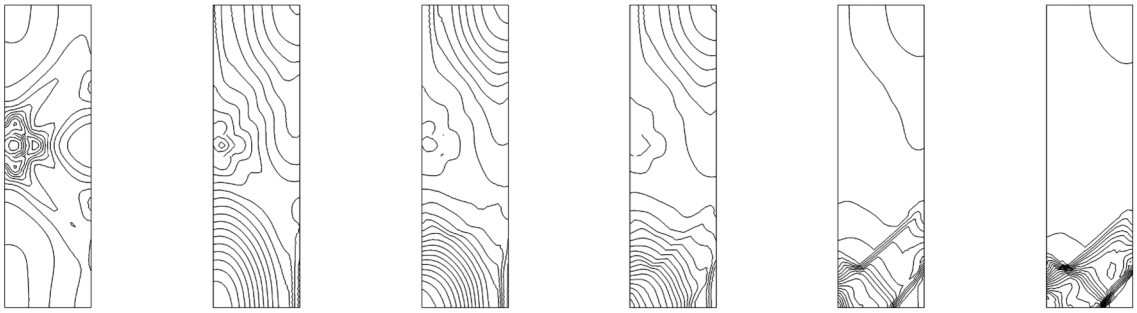

Fig. 15 Evolution of non-local equivalent plastic strains in the specimen during uniaxial compression (non-local model, one initial strong element, $\alpha = 2$, $l = 7.5$ mm, $\varphi = 25°$ and $\psi = 10°$)

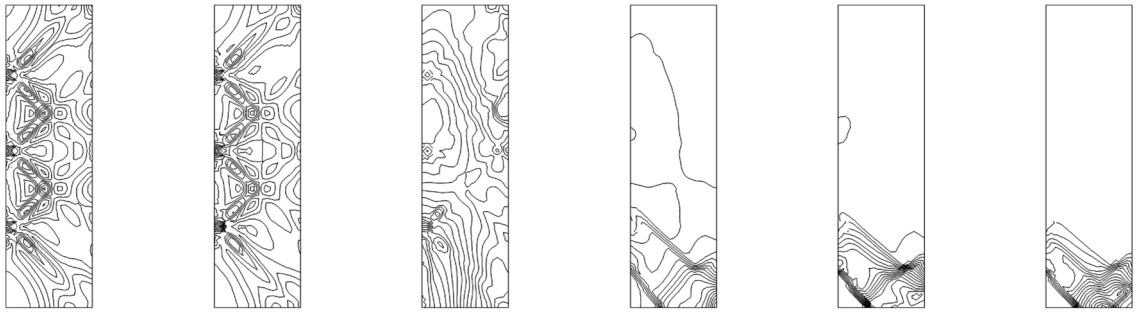

Fig. 16 Evolution of non-local equivalent plastic strains in the specimen during uniaxial compression (non-local model, three initial weak elements, $\alpha = 2$, $l = 7.5$ mm, $\varphi = 25°$ and $\psi = 10°$)

6.2. Effect of imperfections

To investigate the effect of imperfections on the material behaviour during uniaxial plane strain compression, in addition, the simulations were carried out with one initial strong element and few initial weak elements with a different size and spacing.

Fig. 15 presents the results with one strong element in the middle of the left side of the specimen. The location of the shear zone is not connected with the position of the imperfection. The shear zone (reflected from the rigid bottom) is created in the lower part of the specimen.

The evolution of non-local plastic strains in the specimen with three initial weak elements distributed at the same distance along the left side is demonstrated in Fig. 16. Before the peak, two shear zones are created at each week element. The shear zones propagate towards both the top and bottom of the specimen. After the peak, only one shear zone dominates in the whole specimen. The location of this shear zone is, however, different as compared to the results with one weak element at mid-height. The other calculations showed that the size and number of weak elements and distance between them did not influence the thickness and inclination of the shear zone, and the load-displacement curve. Only the location of the shear zone was affected. This result is in contrast to FE-calculations by Shi and Chang (2003) wherein the thickness of a shear zone was influenced by the imperfection spacing.

6.3. Effect of the direction of deformation

Fig. 17 shows the numerical results during uniaxial plane strain extension of the specimen with one weak element at mid-height. Similarly, as during uniaxial compression, the results do not depend on the mesh discretization. The thickness of the shear zone is approximately equal to $L = 1.7$ cm ($2.2 \times l$). Thus, the thickness of the shear zone during extension is smaller by 30% than during compression. The inclination of the shear zone against the bottom is $\Theta = 45.4^{o}$ and 45.2^{o} with a coarse and fine mesh, respectively.

6.4. Effect of characteristic length and non-local parameter

The effect of the parameters α ($\alpha = 2$-5) and l ($l = 2$-12 mm) on the width of shear localization was investigated using the medium mesh (16×56, $\theta = 45^{o}$) during uniaxial compression and extension.

The results show that the larger the parameters l and α, the wider the shear zone L (Table 1). The parameters α and l strongly influence the load-displacement curves in a post-peak regime (Fig. 18). The larger l, the smaller the drop of the curves after the peak. However, they have no influence on the maximum vertical force on the top due to the presence of very smooth horizontal boundaries. The maximum vertical force on the top increases with increasing parameter l only in the case of rough horizontal boundaries (Tejchman and Bobinski 2004). The width of the shear zone L during uniaxial compression (Table 1) can be approximately co-related with the parameters α and l by a following relation:

$$L \cong (1.2 - 1.6)\alpha l \tag{19}$$

However, during uniaxial extension, the width of the shear zone is described by a different relation:

$$L \cong (0.8 - 1.2)\alpha l \tag{20}$$

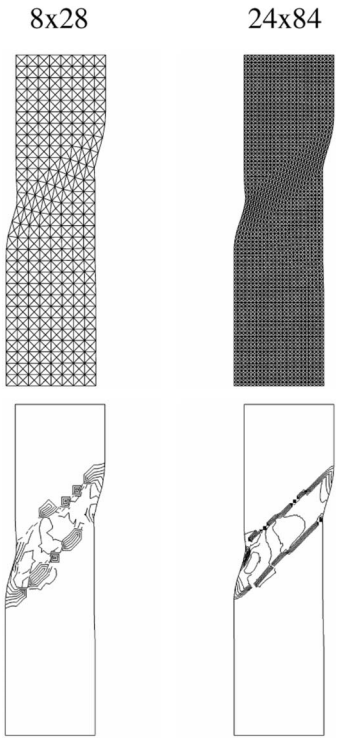

Fig. 17 Deformed meshes and contours of non-local equivalent plastic strains during uniaxial extension (non-local model, $\alpha = 2$, $l = 7.5$ mm, $\varphi = 25^{o}$ and $\psi = 10^{o}$)

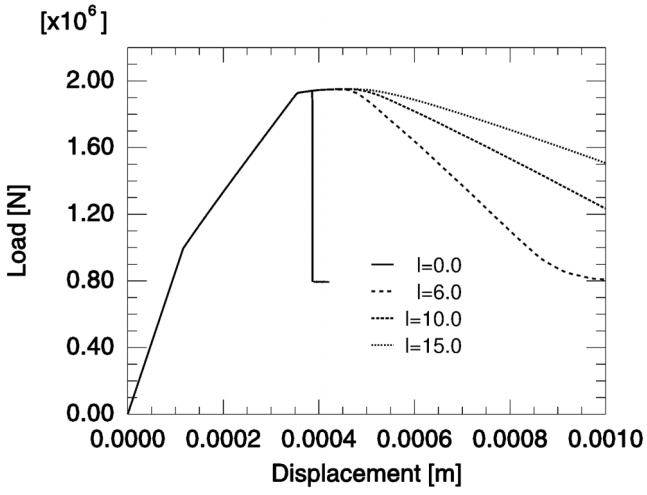

Fig. 18 Load-displacement curves with a different characteristic length (non-local model, $\alpha = 2$, $l = 7.5$ mm, $\varphi = 25^{o}$ and $\psi = 10^{o}$)

Table 1 The calculated width of the shear zone L[cm] during uniaxial compression

L [cm]	α			
	2.0	3.0	4.0	5.0
2	1 element	1.2	1.2	1.5
4	1.4	2.0	2.3	2.5
6	2.1	2.7	3.2	3.6
8	2.7	3.5	4.0	4.7
10	3.2	4.6	diffuse	diffuse
12	3.8	diffuse	diffuse	diffuse

The thickness of the shear zone is obviously dependent upon the boundary conditions of the entire system expressed by e.g., the specimen geometry and loading conditions (Tejchman and Bobinski 2004).

6.5. Effect of the calculation method of non-local plastic strain rates

Figs. 19-21 present the comparative results of FE-simulations (uniaxial compression) using an approximate method by Brinkgreve (1994) (Eq. 15) and an exact method by Strömberg and Ristinmaa (1996) to calculate non-local plastic strain rates $\alpha = 2$, $l = 7.5$ mm, $\theta = 45^{\circ}$, $\varphi = 25^{\circ}$, $\psi = 10^{\circ}$. When plastic strain rates were approximated by total strain rates, the terms $d\varepsilon\,(x + r)$ in Eq. (15) were calculated:

a) in all integration points of the entire body (solution A),
b) in the integration points where only the plastic strains occurred (solution B) and
c) in the integration points where both the plastic strains and softening simultaneously appeared (solution C).

Using an exact iterative method following Strömberg and Ristinmaa (1996), the terms $d\varepsilon_p(x + r)$ in Eq. (13) were computed:

a) in the integration points where only the plastic strains occurred (solution D) or
b) in the integration points where both the plastic strains and softening occurred together (solution E).

The FE-results have shown an insignificant influence of the calculation method of non-local plastic strain rates. The approximate method proposed by Brinkgreve (1994) is less time consuming (by ca. 30%).

6.6. Effect of geometric non-linearity

To investigate the influence of geometric non-linearities on shear localization, the FE-calculations were carried out using both a large- and small-displacement analysis (Abaqus 2001) at a various maximum cohesion yield stress (Fig. 22). The results indicate that the type and location of localized deformation can be different. If the cohesion yield stress at peak is equal to $\sigma_y^{\max} = 32$ MPa, the direction of the shear zone from a large-displacement analysis is various as compared to this from a small-displacement analysis (Fig. 22A) (load-displacement curves and thickness of the shear zone are the same). When the cohesion yield stress at peak is assumed to be larger, $\sigma_y^{\max} = 50$ MPa, one shear zone is obtained using a small-displacement analysis or a buckled specimen is obtained (without the shear zone) using a large-displacement analysis (Fig. 22B).

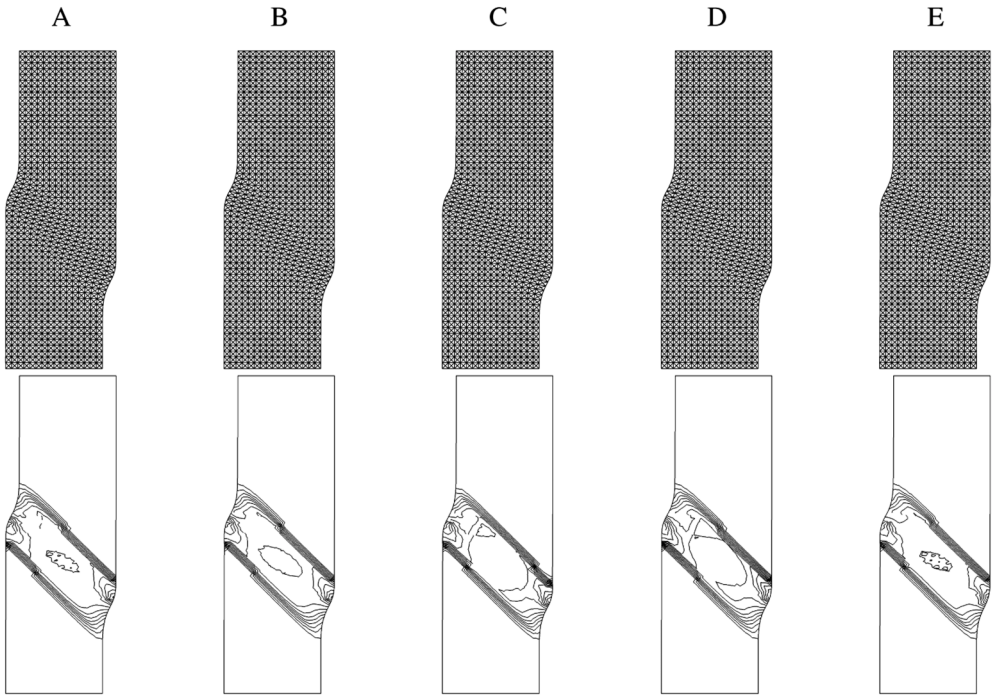

Fig. 19 Deformed meshes and contours of non-local equivalent plastic strains with different calculation methods of ε_p (non-local model, $\alpha = 2$, $l = 7.5$ mm, $\varphi = 25^o$ and $\psi = 10^o$)

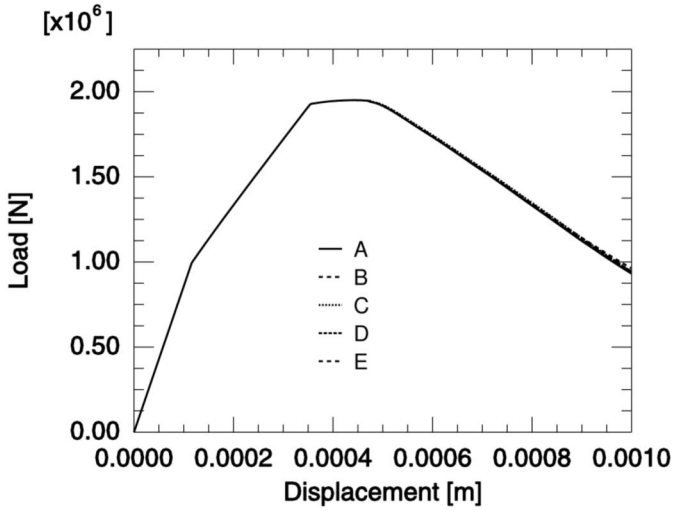

Fig. 20 Load-displacement curves with different calculation methods of ε_p (non-local model, $\alpha = 2$, $l = 7.5$ mm, $\varphi = 25^o$ and $\psi = 10^o$)

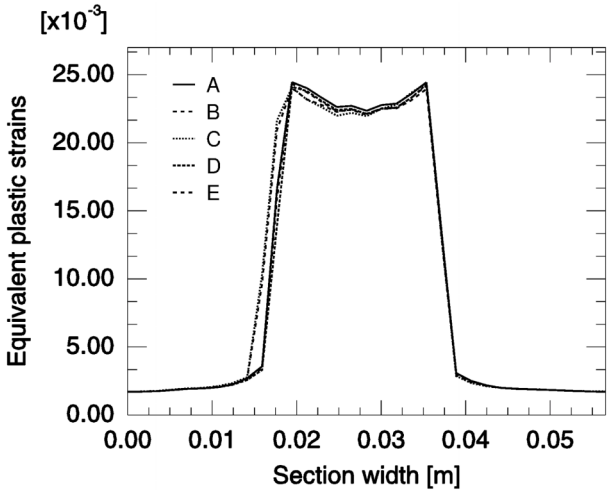

Fig. 21 Distribution of equivalent plastic strains in a shear zone with different calculation methods of ε_p (non-local model, $\alpha = 2$, $l = 7.5$ mm, $\varphi = 25^o$ and $\psi = 10^o$)

7. Conclusions

The FE-calculations on shear localization demonstrate that conventional elasto-plastic models suffer from a mesh-dependency when material softening is included. The thickness and inclination of shear zones inside of a specimen, and load-displacement diagram in a post-peak regime depend strongly upon the mesh discretisation.

An elasto-plastic model with modified non-local softening causes a full regularisation of the boundary value problem during uniaxial compression and extension. Numerical results converge to a finite size of the shear localization upon mesh refinement. The load-displacement curves are similar. The effect of the mesh alignment on the inclination of the shear zone is negligible.

The thickness of the localized shear zone increases with increasing characteristic length and non-local parameter. The thickness of the shear zone during uniaxial compression is larger than during uniaxial extension.

The size and number of imperfections, and the distance between them do not influence the thickness and inclination of the shear zone.

The vertical force on the top increases in the softening regime with increasing characteristic length and non-local parameter. The effect of the characteristic length on the maximum vertical force is noticeable only in the case of very rough boundaries.

The results of a classical non-local theory suffer partly from the mesh sensitivity.

The effect of different calculation methods of non-local plastic strain rates is insignificant.

The consideration of geometric non-linearity influences the type and location of shear localization.

A non-local model can be implemented in commercial finite element codes.

The non-local plastic strain rates can be calculated using an approximate method.

The numerical calculations of strain localization with a non-local model will be continued. To capture the occurrence of cracks (mode I), the so-called smeared crack model with a Rankine condition (de Borst 1988, Sluys 1992, Pamin 1994, Tejchman and Bobinski 2004) will be implemented. The damage elasticity will be taken into account in cracks (Abaqus 2001). The

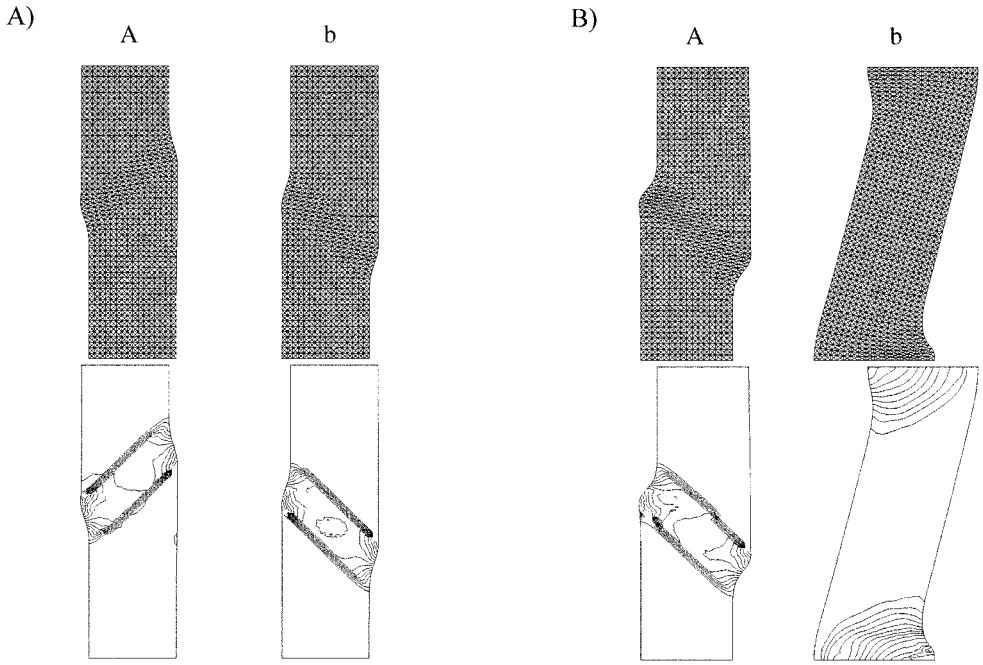

Fig. 22 Deformed meshes and contours of equivalent plastic strains with various cohesion yield stress at peak (non-local model, $\alpha = 2$, $l = 7.5$ mm, $\varphi = 25^{o}$ and $\psi = 10^{o}$): A) $\sigma_y^{max} = 32$ MPa, B) $\sigma_y^{max} = 50$ MPa, a) small-displacement analysis, b) large-displacement analysis

characteristic length will be related to the maximum aggregate size from an inverse identification process of experimental data. Afterwards, a more advanced elasto-plastic model (Menetrey and Willam 1995) to describe more realistically the behaviour of concrete will be used.

References

Abaqus 6.1 Manuals (2001), Hibbitt, Karlsson and Sorensen Inc.

Askes, H. and Sluys, L. J. (2003), "A classification of higher-order strain gradient models in damage mechanics", *Arch. Appl. Mech.*, **53** (5-6), 448-465.

Akkermann J. (2000), "Rotationsverhalten von Stahlbeton-Rahmenecken", *Dissertation*, Universitat Fridericiana zu Karlsruhe, Karlsruhe.

Bazant, Z. P. and Cedolin, L. (1979), "Blunt crackband propagation in finite element analysis", *J. Eng. Mech. Div. ASCE*, **105**(2), 297-315.

Bazant, Z. P. (1986), "Mechanics of distributed cracking", *Appl. Mech. Rev.*, **26**, 675-705.

Bazant, Z., Lin, F. and Pijaudier-Cabot, G. (1987), "Yield limit degradation: non-local continuum model with local strain", (In Owen, ed.)., *Proc. Int. Conf. Computational Plasticity*, Barcelona, 1757-1780.

Bazant, Z. P. and Lin, F. (1988), "Non-local yield limit degradation", *Int. J. Num. Meth. Eng.*, **35**, 1805-1823.

de Borst, R., (1986), "Non-linear analysis of frictional materials", Ph. D. Thesis, Delft University.

de Borst, R., Mühlhaus, H. B., Pamin, J. and Sluys, L. (1992), "Computational modelling of localization of deformation" (In D. R. J. Owen, H. Onate & E. Hinton, eds), *Proc. of the 3rd Int. Conf. Comp. Plasticity*, Swansea: Pineridge Press, 483-508.

Brinkgreve, R. (1994), "Geomaterial models and numerical analysis of softening", *Dissertation*, Delft University, 1-153.

Chen, E. P. (1999), "Non-local effects on dynamic damage accumulation in brittle solids", *Int. J. Num. Anal. Meth. Geomech.* 23: 1-21.
Chen, J., Yuan, H. and Kalkhof, D. (2001), "A nonlocal damage model for elastoplastic materials based on gradient plasticity theory", *Report Nr. 01-13*, Paul Scherrer Institut, 1-130.
Donze, F. V., Magnier, S. A., Daudeville, L., Mariotti, C. and Davenne, L. (1999), "Numerical study of compressive behaviour of concrete at high strain rates", *J. Eng. Mech.*, 1154-1163.
Dragon, A. and Mróz, Z. (1979), "A continuum model for plastic-brittle behaviour of rock and concrete", *Int. J. Eng. Sci.*, **17**.
Eringen, A. C. (1972), "Nonlocal polar elastic continua", *Int. J. Eng. Sci.*, **10**, 1-16.
Eringen, A. C. (1981), "On non-local plasticity", *Int. J. Eng. Sci.*, **19**, 1461-1474.
Ganghoffer, J. F. and de Borst, R. (2000), "A new framework in nonlocal mechanics", *Int. J. Eng. Sci.*, **38**, 453-486.
Herrmann, H. J., Hansen, A. and Roux, S. (1989), "Fracture of disordered elastic lattices in two dimensions", *Physical Rev. B*, **39**, 637-647.
Hilleborg, A. (1985), "The theoretical basis of a method to determine the fracture energy of concrete", *Materials and Structures,* **18**, 291-296.
Hughes T. J. R. and Winget J. (1980), "Finite rotation effects in numerical integration of rate constitutive equations arising in large deformation analysis", *Int. J. Num. Methods Eng.*, **15**, 1862-1867.
Ibrahimbegovic, A., Markovic, D. and Gatuingt, F. (2003), "Constitutive model of coupled damage-plasticity and its finite element implementatation", *Eur. J. Finite Elem.*, **12**(4), 381-405.
Jirasek, M.and Rolshoven, S. (2003), "Comparison of integral-type nonlocal plasticity models for strain-softening materials", *Int. J. Eng. Sci.*, **41**, 1553-1602.
Lade, P. V. and Jakobsen, K. P. (2002), "Incrementalization of a single hrdening constitutive model for frictional materials", *Int. J. Numer. Anal. Methods in Geomech.*, **26**, 647-659.
Lemaitre, J. (1985), "Coupled elasto-plasticity and damage constitutive equations", *Comput. Meth. Appl. Mech. Eng.*, **51**, 31-49.
Loret B. and Prevost J. H. (1990), "Dynamic strain localisation in elasto-visco-plastic solids, Part 1. General formulation and one-dimensional examples", *Comput. Meth. Appl. Mech. Eng.*, **83**, 247-273.
Maier, T. (2002), "Numerische Modellierung der Entfestigung im Rahmen der Hypoplastizität", Ph. D. Thesis, University of Dortmund.
Maier, T. (2003), "Nonlocal modelling of softening in hypoplasticity", *Comput. Geotech.* **30** (7), 599-610.
Marcher, T. and Vermeer, P. A. (2001), "Macro-modelling of softening in non-cohesive soils" (In P. A. Vermeer *et al.* eds), *Continuous and Discontinuous Modelling of Cohesive-Frictional Materials*, Springer-Verlag, 89-110.
Meftah, F. and Reynouard, J. M. (1998), "A multilayered mixed beam element on gradient plasticity for the analysis of localized failure modes", *Mechanics of Cohesive-Frictional Materials*, **3**, 305-322.
Menetrey, P. H. and Willam, K. J. (1995), "Triaxial failure criterion for concrete and its generalization", *ACI Struct. J.*, 311-318.
Mühlhaus, H. B. (1986), "Scherfugenanalyse bei Granularen Material im Rahmen der Cosserat-Theorie", *Ingen. Archiv*, **56**, 389-399.
Mühlhaus, H. B. and Aifantis, E. C. (1991), "A variational principle for gradient plasticity", *Int. J. Solids Struct.*, **28**, 845-858.
Ortiz, M. and Simo, I. C. (1986), "An analysis of a new class of integration algorithms foe elastoplastic constitutive relation", *Int. I. Num. Meth. in Eng.*, **23**, 353-366.
Pamin, J. (1994), "Gradient-dependent plasticity in numerical simulation of localization phenomena", Ph. D. Thesis, University of Delft.
Pamin, J. and de Borst, R. (1998), "Simulation of crack spacing using a reinforced concrete model with an internal length parameter", *Arch. Appl. Mech.*, **68** (9), 613-625.
Peerlings, R. H. J., de Borst, R., Brekelmans, W. A. M. and Geers, M. G. D. (1998), "Gradient enhanced damage modelling of concrete fracture", *Mech. Cohes.-Friction. Mater.*, **3**, 323-342.
Pijaudier-Cabot, G. and Bazant, Z. P. (1987), "Nonlocal damage theory", *ASCE J. Eng. Mech.*, **113**, 1512 -1533.
Pijaudier-Cabot, G. (1995), "Non local damage", *Continuum Models for Materials with Microstructure* (In H. B. Mühlhaus, ed.), John Wiley & Sons Ltd.
Pietruszczak, S., Jiang, J. and Mirza, F. A. (1988), "An elastoplastic constitutve model for concrete", *Int. J.*

Solids Struct., **24** (7), 705-722.
Place, D. and Mora, P. (2001), "A random lattice solid model for simulation of fault zone dynamics and fracture processes" (In H. B. Mühlhaus *et al*. Eds.), *Bifurcation and Localisation Theory in Geomechanics,* 321-333.
di Prisco, M. and Mazars, J. (1996), "Crush-crack-a non-local damage model for concrete", *Mechanics of Cohesive-Frictional Materials*, **1**, 321-347.
di Prisco, C., Imposimato, S. and Aifantis, E. C. (2002), "A visco-plastic constitutive model for granulr soils modified according to non-local and gradient approaches", *Int. J. Numer. Anal. Meth. Geomech*., **26**, 121-138.
Ragueneau, F., Borderie, Ch. and Mazars, J. (2000), "Damage model for concrete-like materials coupling cracking and friction", *Int. J. Num. Anal. Meth. Geomech.* **5**, 607-625.
Sakaguchi, H. and Mühlhaus, H. B. (1997), "Mesh free modelling of failure and localisation in brittle materials", *Deformation and Progressive Failure in Geomechanics* (In A. Asaoka, T. Adachi and F. Oka eds.), 15-21.
Schanz, T. (1998), "A constitutive model for cemented sands", *Localisation and Bifurcation Theory for Soils and Rocks* (In Adachi, Oka and Yashima eds.), Balkema, Rotterdam, 165-172.
Shi, Q., Chang, C. S. (2003), "Numerical analysis for the effect of heterogeneity on shear band formation", *Proc. 16th ASCE Eng. Mech. Conf.,* University of Washington, Seattle, 1-11.
Sluys, L. J. (1992), "Wave propagation, localisation and dispersion in softening solids", *Dissertation*, Delft University of Technology, Delft.
Sluys, L.J. and de Borst, R. (1994), "Dispersive properties of gradient and rate-dependent media", *Mech. Mater.* **183**, 131-149.
Strömberg, L. and Ristinmaa, M. (1996), "FE-formulation of nonlocal plasticity theory", *Comput. Meth. Appl. Mech. Eng*,. **136**, 127-144.
Tejchman, J. and Wu, W. (1993), "Numerical study on patterning of shear bands in a Cosserat continuum", *Acta Mechanica*, **99**, 61-74.
Tejchman, J., Herle, I. and Wehr, J. (1999), "FE-Studies on the influence of initial void ratio, pressure level and mean grain diameter on shear localisation", *Int. J. Num. Meth. Geomech.*, **23**, 2045-2074.
Tejchman, J. (2003), "A non-local hypoplastic constitutive law to describe shear localisation in granular bodies", *Arch. Hydro-Engineering and Environmental Mech.*, **50** (4), 229-250.
Tejchman, J. (2004), "Comparative FE-studies of shear localizations in granular bodies within a polar and non-local hypoplasticity", *Mech. Res. Comm.* **31** (3), 341-354.
Tejchman, J. and Bobinski, J. (2004), "Non-local elasto-plastic model to simulate localization of deformation in concrete", *Lecture during the Int. Conf. SEMC 2004*, Cape Town, South Africa, 5-7.07.2004.
Willam, K. J. and Warnke, E. P. (1975), "Constitutive model for the triaxial behaviour of concrete", *IABSE Seminar on Concrete Structures subjected to Triaxial Stress*, Bergamo, Italy, 1-31.
Vervuurt, A., van Mier, J. G. M. and Schlangen, E. (1994), "Lattice model for analyzing steel-concrete interactions", *Comp. Meth. Geomech.* (In Siriwardane and Zaman eds.), 713-718, Balkema, Rotterdam.
Zbib, H. M. and Aifantis, C. E. (1989), "A gradient dependent flow theory of plasticity: application to metal and soil instabilities", *Appl. Mech. Reviews*, **42** (11), 295-304.
Zhou, W., Zhao, J., Liu, Y. and Yang, Q. (2002), "Simulation of localization failure with strain-gradient-enhanced damage mechnics", *Int. J. Numer. Anal. Meth. Geomech.* **26**, 793-813.

CC